Pathological α-syn aggregation is mediated by glycosphingolipid chain length and the physiological state of α-syn in vivo

Kristina Fredriksen[a], Stefanos Aivazidis[a], Karan Sharma[a], Kevin J. Burbidge[a], Caleb Pitcairn[a], Friederike Zunke[a,b], Eilrayna Gelyana[a], and Joseph R. Mazzulli[a,1]

[a]The Ken and Ruth Davee Department of Neurology, Northwestern University Feinberg School of Medicine, Chicago, IL 60611; and [b]Department of Molecular Neurology, University Hospital Erlangen, Friedrich-Alexander University Erlangen-Nuremberg, Erlangen 91054, Germany

Edited by Hugo Bellen, Department of Molecular and Human Genetics and Neuroscience, Baylor College of Medicine, Houston, TX; received May 5, 2021; accepted October 25, 2021

GBA1 **mutations that encode lysosomal β-glucocerebrosidase (GCase) cause the lysosomal storage disorder Gaucher disease (GD) and are strong risk factors for synucleinopathies, including Parkinson's disease and Lewy body dementia. Only a subset of subjects with *GBA1* mutations exhibit neurodegeneration, and the factors that influence neurological phenotypes are unknown. We find that α-synuclein (α-syn) neuropathology induced by GCase depletion depends on neuronal maturity, the physiological state of α-syn, and specific accumulation of long-chain glycosphingolipid (GSL) GCase substrates. Reduced GCase activity does not initiate α-syn aggregation in neonatal mice or immature human midbrain cultures; however, adult mice or mature midbrain cultures that express physiological α-syn oligomers are aggregation prone. Accumulation of long-chain GSLs (≥C22), but not short-chain species, induced α-syn pathology and neurological dysfunction. Selective reduction of long-chain GSLs ameliorated α-syn pathology through lysosomal cathepsins. We identify specific requirements that dictate synuclein pathology in GD models, providing possible explanations for the phenotypic variability in subjects with GCase deficiency.**

lysosomal storage disease | glycosphingolipids | α-synuclein | Gaucher disease | Parkinson's disease

Gaucher disease (GD) is a lysosomal storage disorder caused by loss-of-function mutations in the *GBA1* gene that encodes lysosomal β-glucocerebrosidase (GCase). GCase degrades glycosphingolipids (GSLs), including glucosylceramides (GluCers), into glucose and ceramide, and GCase mutations result in the accumulation of GluCer in lysosomes of various tissues. Heterozygote carriers of the same loss-of-function GCase mutations are estimated to be at 5- to 10-fold higher risk for developing Parkinson's disease (PD) or Lewy body dementia (1). In GD, significant variability exists in the clinical and pathological presentation, resulting in three main GD subtypes (2). Type 1 GD is characterized by visceral abnormalities, including enlarged liver and spleen and bone marrow dysfunction, leading to thrombocytopenia but without neurodegeneration and α-synuclein (α-syn) pathology (3). Types 2 and 3 demonstrate similar visceral symptoms but with additional extensive neuronal loss, α-syn pathology in the form of classical Lewy bodies, and neurological dysfunction (3, 4). As life expectancy of type 1 GD has increased because of enzyme replacement therapy, a higher percentage of patients develop PD symptoms with age (5), suggesting that aging could contribute to the penetrance of *GBA1* mutations. The dramatic phenotypic heterogeneity suggests that GD is not a simple, monogenic disease but a complex disorder that is influenced by both genetic and nongenetic modifiers. Although the factors that contribute to clinical and pathological variability in GD are not known, genetic modifiers have been identified that associate with GD severity, including CLN8 and SCARB2 (6, 7). Within PD patients that harbor *GBA1* mutations (GBA-PD), the search for genetic modifiers has shown that synergism may exist with the *SNCA* gene that encodes α-syn and *CTSB* that encodes lysosomal cathepsin B (8). Variants in lysosomal cathepsins could influence the severity of α-syn accumulation, since, under physiological or pathological conditions, α-syn can be degraded by the lysosome (9–11) and is a direct substrate of cathepsin B and L (12).

An additional factor that may contribute to phenotypic variability in GD is the accumulation of specific GluCer subtypes with particular acyl chain lengths. GluCer and other GSLs exist as a family of lipid isoforms differentiated by the length of the *N*-acyl fatty acid moiety linked to the sphingoid base. GluCer chains range from C14 to C26 in the brain; however, C18 and C24:1 are the predominant species (13). Studies of neuronopathic GD (nGD) brain or mouse models showed intraneuronal accumulation of multiple GluCer species that correlated with neuroinflammation (14–19), and some cases demonstrate selective accumulation of long-chain GluCers in nGD (20). Our recent work in PD patient midbrain neurons showed that inhibition of wild-type (wt) GCase, caused by α-syn, resulted in the selective accumulation of long-chain-length GluCers, including C22 and C24:1, while C14, 16, and C18 were unchanged (21). Together, these data indicate that GluCer accumulation plays

Significance

Gaucher disease (GD) is a glycosphingolipid (GSL) lysosomal storage disorder that displays a wide spectrum of clinical manifestations, including the presence or absence of neurological symptoms. GD-causing mutations in β-glucocerebrosidase are also associated with synucleinopathies, including Parkinson's disease, but with incomplete penetrance. Our data indicates that accumulation of long-chain GSLs (≥C22) is critically important for inducing α-synuclein neuropathology in vivo. Reducing long-chain GSLs by 30 to 40% was sufficient to prevent or reverse α-synuclein neuropathology but only in the presence of fully functional cathepsins. Our work offers mechanistic insight into the factors that drive neurodegenerative phenotypes in GD and suggests that GSL-reducing therapies require functional cathepsins to effectively reduce pathological α-synuclein and prevent neurodegeneration.

Author contributions: K.F. and J.R.M. designed research; K.F., S.A., K.S., K.J.B., C.P., F.Z., E.G., and J.R.M. performed research; K.F., S.A., K.S., K.J.B., C.P., F.Z., E.G., and J.R.M. analyzed data; and J.R.M. wrote the paper.

The authors declare a competing interest. J.R.M. is a scientific co-founder of Lysosomal Therapeutics, INC.

This article is a PNAS Direct Submission.

[1]To whom correspondence may be addressed. Email: jmazzulli@northwestern.edu.

This article contains supporting information online at http://www.pnas.org/lookup/suppl/doi:10.1073/pnas.2108489118/-/DCSupplemental.

Published December 6, 2021.

an important role in neurodegeneration induced by *GBA1* mutations; however, the specific contributions of distinct GluCer species have not been examined.

Here, we extend our studies on the role of GSLs in α-syn aggregation to further define conditions that are required to induce pathology and neurological dysfunction. We previously showed that α-syn exists as monomers and high–molecular weight (HMW) oligomers under physiological conditions in human midbrain cultures (22). In vitro, we found that GluCer mildly induced aggregation of α-syn monomers but primarily acted on physiological oligomers to convert them into toxic oligomers and fibrillar inclusions (22). α-syn accumulation can be prevented or reversed by reducing GSLs with GluCer synthase inhibitors (GCSi) in both GD and PD patient cultures, as well as in mouse models (22–24). While this work suggests a close relationship between GCase function and α-syn pathology, additional factors must exist that create a permissive environment for α-syn accumulation. Indeed, studies that used newborn mice or embryonic primary neuron cultures treated with the GCase inhibitor, conduritol beta epoxide (CBE), have shown no changes in α-syn despite reduced GCase activity (25–27). However, other studies that use matured neuron cultures, neuronal cell lines, or adult mice have shown that CBE dramatically induces α-syn aggregates (22, 28–31). We used an in vivo GD model and induced pluripotent stem cell (iPSC)–-derived patient midbrain cultures to identify specific conditions that are required to induce α-syn pathology, providing possible explanations for the variable neurological penetrance in patients that harbor *GBA1* mutations.

Results

GSL Accumulation Has No Effect on α-syn in Neonatal Mice. Our previous studies showed that GSLs initiate α-syn aggregation by converting HMW physiological oligomers into assembly state intermediates (22). To determine if GSLs initiate α-syn accumulation in vivo through a similar mechanism, we employed a pharmacological mouse model that involves inhibition of GCase by intraperitoneal (i.p.) injection of CBE. The CBE mouse model is well established, and has been used extensively to induce GSL accumulation in the brain and model other features of GD (32–34). The model allows for the study of reduced GCase activity in the absence of *GBA1* mutations and facilitates precise control over the initiation of GSL accumulation in animals of different ages. Furthermore, it dramatically facilitates the temporal correlation of individual α-syn species with GSL levels and neural injury. Recent studies have shown that neonates (<2 wk of age) accumulate GSLs more severely compared to older animals upon CBE treatment (34). Therefore, we treated wt mice at postnatal day 8 (P8) for 7 d with 100 mg/kg CBE through i.p. injection. To measure α-syn, we used multiple α-syn antibodies that either detect total endogenous mouse α-syn (C20) or preferentially detect pathogenic α-syn formed upon GSL accumulation (e.g., syn505) (22). Surprisingly, we found that α-syn levels were unchanged in brain lysates, despite a 95% reduction in GCase activity, and dramatic 10-fold elevation in GluCer and 100-fold elevation in glucosylsphingosine (GluSph) levels (Fig. 1 *A* and *B*). The levels of the related sphingolipid galactosylceramide were unaltered, demonstrating the specificity of CBE (Fig. 1*A*). Since our previous culture studies showed that soluble HMW oligomers were primarily affected by GSLs (22), we next analyzed soluble lysates by nondenaturing size-exclusion chromatography (SEC)/Western blot. We found that the levels of oligomeric α-syn eluting as a 100-Å–sized protein were almost undetectable in vehicle-treated mice and that CBE had no effect on oligomer levels. Probing with either the C20 or syn505 antibodies both showed no change with CBE treatment (Fig. 1*C*). These data indicate that depletion of GCase activity and substrate accumulation do not influence α-syn aggregation in neonatal mice in vivo.

GSL Accumulation Initiates the Conversion of Physiological α-syn Oligomers into Pathogenic Species in Adult Mice. Since previous studies showed that CBE could induce α-syn accumulation in adult mice (29, 30), we next treated older (90 d) wt mice with CBE for 7 d via i.p. injection. As expected, CBE injection resulted in a dramatic reduction in GCase activity in the brain and a fourfold elevation of GluCer compared to vehicle-injected mice (Fig. 2*A*). In contrast to neonatal mice, adult mice showed a highly reproducible two- to threefold elevation of insoluble α-syn detected in cortical extracts with antibody C20 or syn505 (Fig. 2*B*). Thus, despite depletion of GCase activity and severe GluCer accumulation in both neonates and adult brain, only adult mice demonstrate α-syn accumulation upon CBE treatment.

We then compared healthy, untreated neonate and adult mouse brains to explain the differential response to CBE. Since α-syn aggregation is heavily dependent on protein concentration in vivo and in vitro (35–37), we first compared total α-syn protein levels in healthy 15- and 90-d-old mice. However, we found that 15- and 90-d-old mice expressed equal amounts of α-syn (*SI Appendix*, Fig. S1*A*). Next, we assessed lysosomal protease activity, since physiological α-syn can be degraded by lysosomes (9). This showed that 90-d-old mice had elevated activity (*SI Appendix*, Fig. S1*B*), indicating that vulnerability to GSLs was not due to decreased lysosomal activity. We then compared the levels of physiological oligomers of α-syn, since our previous studies showed that GSLs primarily interact with these species (22). SEC analysis showed that 90-d-old healthy mice had dramatically higher-oligomer levels that averaged at around 20% of the total α-syn, as compared to healthy neonates that expressed 1 to 5% oligomers (*SI Appendix*, Fig. S1*C*). These data indicate that physiological α-syn oligomers increase with age in mouse brain, and their levels correlate with sensitivity to CBE-induced α-syn aggregation.

We next sought to determine if similar, age-dependent changes in α-syn occur in human iPSC-derived neurons. We differentiated iPSCs from healthy controls into midbrain dopamine neurons and allowed them to mature in vitro for either 30 or 120 d. Our previous studies showed that iPSC-derived neurons at day 30 exhibit many properties of midbrain neurons but are not fully mature (38). However, aging cultures for 60 to 120 d in vitro permits the development of neurons that are more mature, as exhibited by extensive, β-iii-tubulin–positive neurite networks and synapsin expression within synapses (38). Similar to mouse brain, SEC analysis indicated that immature iPSC neurons predominantly expressed α-syn monomers, while neurons matured to day 120 expressed both oligomers and monomers (*SI Appendix*, Fig. S1*D*). CBE treatment in day 120 cultures resulted in a dramatic elevation of insoluble α-syn (*SI Appendix*, Fig. S1*E*), consistent with our previous findings (22). However, CBE had no effect on α-syn aggregation in immature day 30 cultures, since all of the α-syn remained soluble (*SI Appendix*, Fig. S1*E*). Collectively, our studies suggest that neuronal maturity and/or the presence of physiological α-syn oligomers renders neurons vulnerable to GSL accumulation, resulting in pathological aggregation.

Temporal Correlation of GCase Activity, GSLs, and Distinct α-syn Species In Vivo. Having established that GSLs induce α-syn aggregation in adult mice, we next sought to determine the kinetic relationship between reduced GCase activity, elevated GSL substrates, and distinct α-syn species in vivo. Upon CBE injection, brain GCase activity dramatically decreased within 2 d followed by a slower exponential decline between 2 and 7 d. GSL substrates, including GluCer and GluSph, increased linearly over the 7-d period (Fig. 2*C*). Sequential extractions

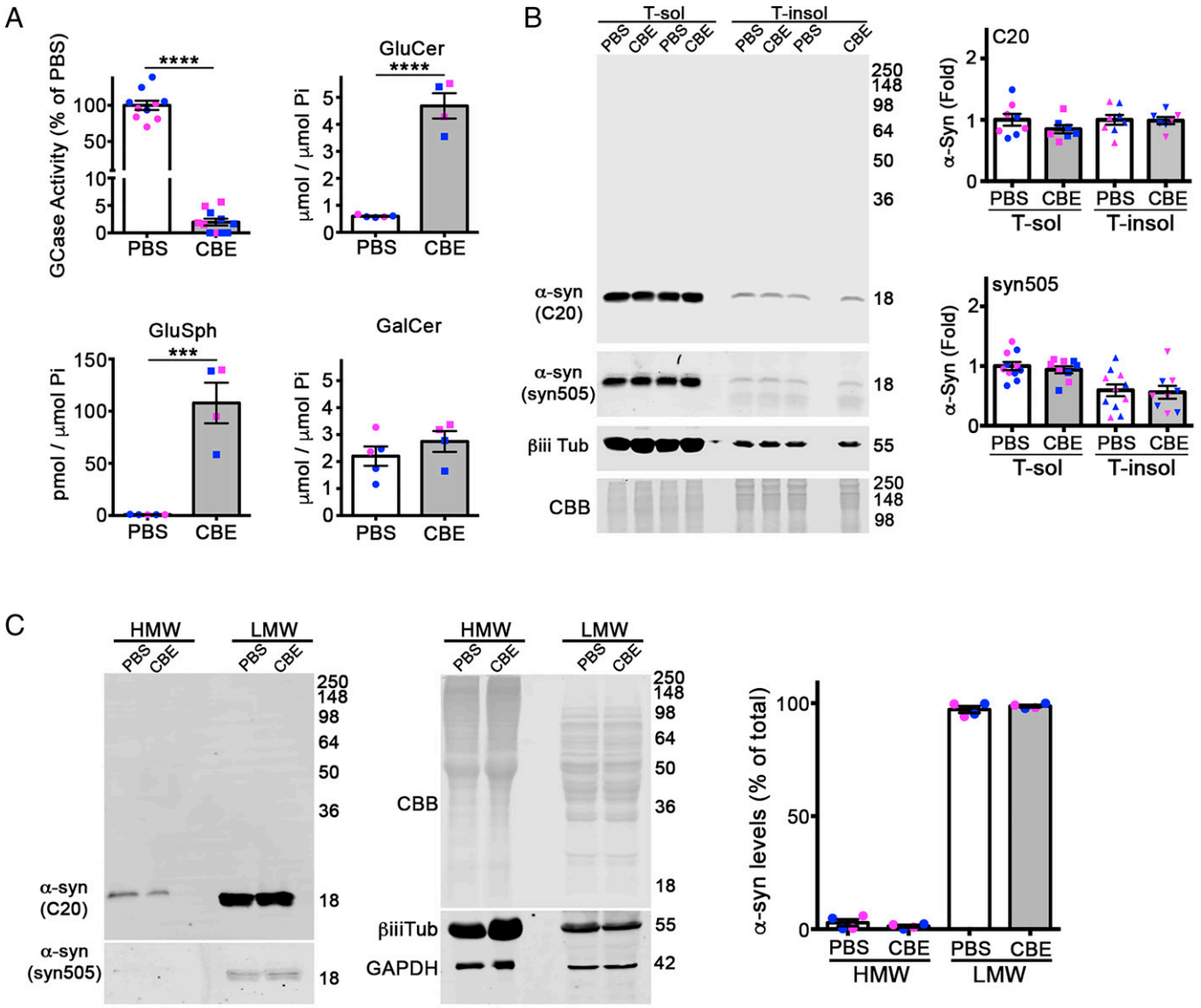

Fig. 1. Reduced GCase activity does not influence α-syn aggregation in neonatal mice. (*A*) The wt mice at P8 were i.p. injected with CBE at 100 mg/kg for 7 d, and cortex was analyzed for GCase activity and GSLs substrates (GluCer and GluSph). Galactosylceramide (GalCer) was analyzed as a specificity control. Lipids were normalized to inorganic phosphate (Pi). (*B*) Whole brains were sequentially extracted and separated into triton X-100 soluble (T-sol) and insoluble (T-insol) fractions followed by Western blot for α-syn. β-iii-tubulin and Coomassie Brilliant Blue (CBB) were used as a loading controls. Quantifications are shown on the right normalized to CBB. C20 (rabbit) and syn505 (mouse) were sequentially probed on the same blot using two different, fluorescent secondary antibodies. (*C*) T-sol lysates were analyzed by SEC/Western blot to reveal the levels of HMW oligomers and low–molecular weight (LMW) monomers of α-syn. CBB, β-iii-tubulin, and GAPDH are loading controls. Quantification is on the right. Values are the mean ± SEM; Student's *t* test was use for each phosphate-buffered saline (PBS) versus CBE comparison, $****P < 0.0001$; $***P < 0.001$. Each plot shown represents an individual mouse (pink, female; blue, male).

showed that soluble α-syn was depleted, while insoluble α-syn increased between 4 and 7 d post-CBE, subsequent to GSL accumulation (Fig. 2*D*). Soluble α-syn oligomers isolated by SEC and detected with C20 accumulated concomitantly with GSLs at 2 and 4 d, followed by their depletion at day 7, suggesting that they are likely intermediates consumed into insoluble aggregates (Fig. 2*E*). Interestingly, we observed a decline in soluble monomers that paralleled the increase in oligomers, which indicates that monomers were likely rapidly consumed into oligomeric species at a rate that surpassed the synthesis of newly made α-syn (Fig. 2*E*). Quantification of soluble oligomeric fractions with syn505 showed a rapid increase in SDS/heat stable species migrating between 30 and 148 kDa by SDS–polyacrylamide gel electrophoresis (PAGE) that occurred early in the aggregation process at 2 d post-CBE and were sustained throughout treatment (Fig. 2*F*). Oligomeric fractions isolated by SEC were further analyzed with conformational antibodies including OC, which detects in-register β-sheet oligomers, and A11, which detects out-of-register β-sheet oligomers (39–41). Importantly, A11-reactive oligomers are well characterized and associated with toxicity (39). Similarly, OC-reactive species are known as "fibrillar oligomers" and are thought to be precursors to insoluble amyloid fibrils. We found that A11-type oligomers accumulated subsequent to GSLs, while OC-type oligomers transiently increased at day 4 followed by their rapid depletion at day 7 (Fig. 2*G*). Similar to C20-reactive oligomers, this suggests that OC-type oligomers become consumed into insoluble aggregates between 4 and 7 d post-CBE. These data indicate that CBE treatment initially induces the accumulation of soluble oligomers followed by

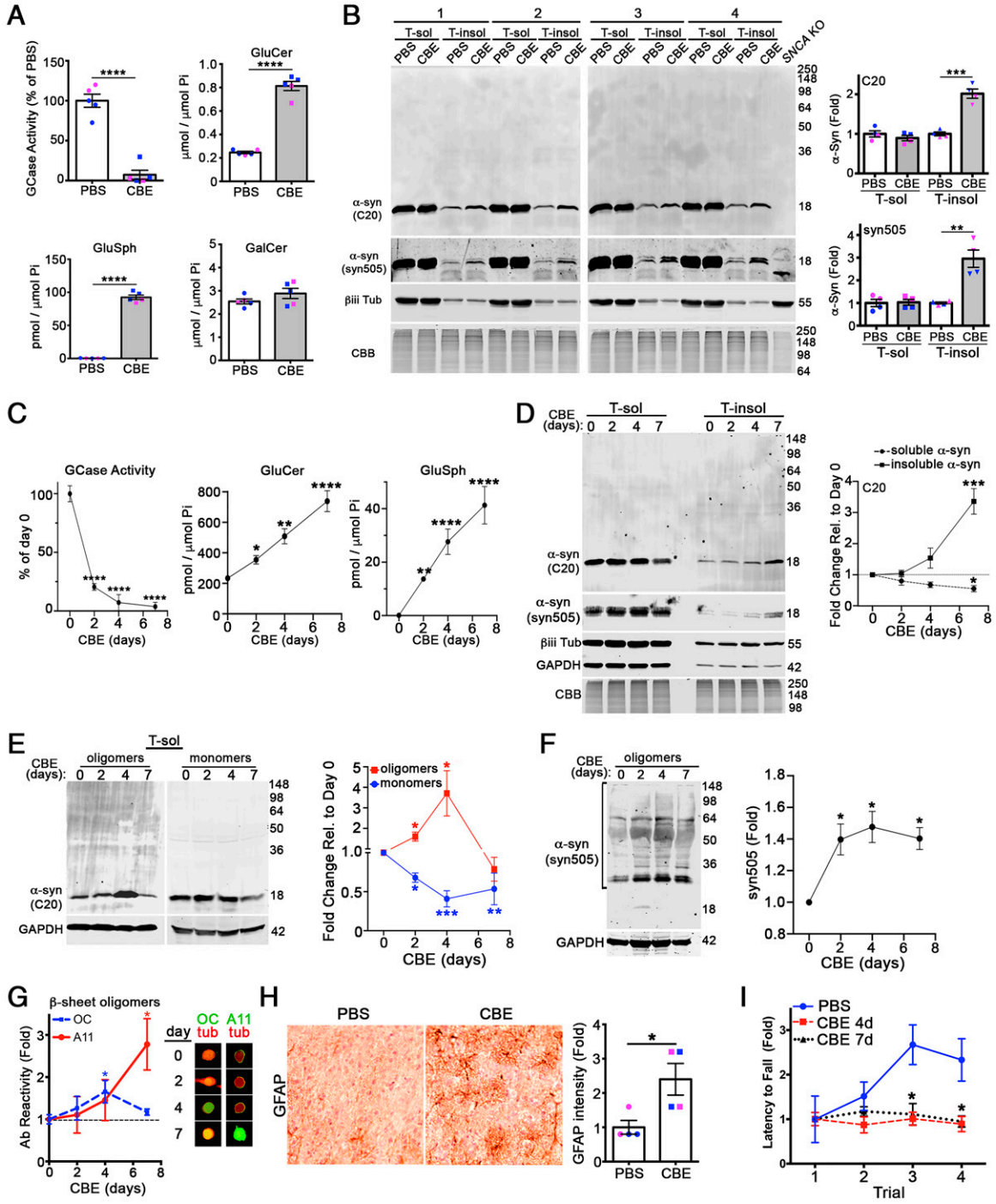

Fig. 2. Reduced GCase activity initiates α-syn aggregation in adult mice. (*A*) The wt mice at P90 were i.p. injected with CBE at 100 mg/kg for 7 d, and cortex was analyzed for GCase activity and GSLs substrates (GluCer and GluSph). Galactosylceramide (GalCer) was analyzed as a specificity control. Lipids were normalized to inorganic phosphate (Pi). (*B*) Cortex was sequentially extracted and separated into triton X-100 soluble (T-sol) and insoluble (T-insol) fractions followed by Western blot for α-syn. C20 (rabbit pAb) and syn505 (mouse mAb) were sequentially probed on the same blot and detected with distinct secondary antibodies. β-iii-tubulin and Coomassie Brilliant Blue (CBB) were used as loading controls. Quantifications are shown on the right normalized to CBB. Data from four individual mice are shown. (*C*) Time course analysis of 90-d-old mice injected with CBE shows gradual accumulation of GluCer substrates ($n = 4$). (*D*) Sequential extraction/Western blot was done as in *B* ($n = 4$). C20 signal is quantified to the right. (*E*) SEC/Western blot analysis of T-sol lysates was done to reveal the levels of oligomers and monomers of α-syn over time. GAPDH is a loading control. Quantification is on the right ($n = 3$). (*F*) Oligomers were reprobed using syn505 that preferentially detects pathogenic α-syn, quantified on the right ($n = 4$). (*G*) Soluble lysates were dot blotted with conformational antibodies that detect in-register (OC) or out of register (A11) β-sheet structures ($n = 4$). Quantification was expressed as fold change compared to day 0 and normalized to tubulin. A representative image is shown to the right (A11 or OC, green; tubulin, red). (*H*) Immunohistochemical analysis of the cortex of CBE-treated mice compared to phosphate-buffered saline (PBS) vehicle controls. (*I*) Rotarod performance was tested in mice injected with CBE at 0, 4 (red dashed), or 7 d (black dotted) ($n = 4$). The same group of mice were used throughout the study and assessed at different time points. Values are the mean ± SEM; Student's *t* test was used for *A*, *B*, and *H*; ANOVA with Dunnett's post hoc test was used for *C*–*G*, and *I*, using day 0 as a control; $^{*}P < 0.05$, $^{**}P < 0.01$, $^{***}P < 0.001$, and $^{****}P < 0.0001$. Each plot shown represents an individual mouse (pink, female; blue, male).

insoluble aggregates. Analysis of SEC-isolated oligomers shows that CBE induced at least two oligomer subtypes distinguished by their conformation, consumption into insoluble aggregates (C20 and OC type), or their persistence in the soluble fraction (syn505 and A11 type).

We next assessed astrogliosis by GFAP immunostaining in the same cortical area that was analyzed biochemically to assess neuronal injury. This showed an elevation of astrogliosis in CBE-treated mice by day 7 (Fig. 2*H*). Neurological function was assessed by behavioral studies using the rotarod test. This revealed a reduction in rotarod performance at 4 and 7 d post-CBE (Fig. 2*I*). Together, these data demonstrate an association of GSL accumulation, α-syn pathology, neuronal injury, and dysfunction. The correlation of syn505- and A11-type oligomers with astrogliosis and reduced rotarod performance further suggests their involvement in GSL-induced neurotoxicity.

Reducing Long-Chain GluCers Prevents the Initial Conversion of α-syn into Pathogenic Species. We next sought to determine the role of specific GluCer species in pathogenesis. Previous studies showed that the brain penetrant GCSi, venglustat (42), selectively reduced long-chain sphingolipids with >21 carbon chain lengths but did not affect short-chain GluCers in CBE-injected mice (43). Therefore, we coinjected 90-d-old mice with CBE and venglustat to specifically prevent the accumulation of long-chain GluCers. We found that GCase activity remained depleted in CBE + GCSi–cotreated mice, and long-chain GluCers (C22 and C24) were reduced, while short-chain GluCers (C14, C16, C18, C20, and C20:1) and GluSph were not significantly changed (Fig. 3 *A* and *B* and *SI Appendix*, Fig. S2). Soluble α-syn did not change, however analysis of insoluble α-syn showed a mild but significant reduction of 12% with α-syn antibody C20 that detects total α-syn (Fig. 3 *C* and *D*). To validate our results, we sequentially probed the blots syn505 and syn303, which preferentially detects pathological α-syn conformations (44). Probing with syn505 showed a reduction of 25%, while syn303 showed a 30% reduction (Fig. 3 *C* and *D*). This demonstrates that GSL reduction reduces pathological α-syn and is consistent with previous findings in other GD models (23).

Since we observed mouse-to-mouse variation with respect to the degree of GluCer reduction within the CBE + GCSi group, we correlated the level of each GluCer isoform with the amount of insoluble α-syn for each individual mouse using syn303. This revealed a positive correlation between long-chain and desaturated GluCers with α-syn, in which C24:1 and C26 showed the strongest relationship (Fig. 3*E* and *SI Appendix*, Fig. S2). Even though GluCers C22:1, C24:1, C26, and C26:1 were not significantly reduced by GCSi as a group (*SI Appendix*, Fig. S2), we found that mice with the lowest levels of these particular GluCers also had the lowest levels of insoluble α-syn (Fig. 3*E* and *SI Appendix*, Fig. S2). No correlation was observed with other GluCers, with the exception of C18:1, which showed a mild positive correlation (*SI Appendix*, Fig. S2). These data indicate that preventing the accumulation of long-chain GluCers can reduce α-syn pathology. Short-chain GluCers or GluSph were not significantly reduced and did not correlate with pathological α-syn, suggesting that they are not involved in initiating α-syn aggregation in vivo.

Both physiological- and pathological-type oligomers elute at the same fraction by SEC corresponding to a 100-Å radius–sized protein (22). However, GSL-induced oligomers are extremely stable in 0.1% SDS, while physiological species readily break down into monomers (22). To determine if reduction of long-chain GluCers prevented the formation of pathogenic oligomers, we treated cortical lysates with SDS to eliminate physiological oligomers, then measured GSL-stabilized oligomers by SEC. The oligomers extracted from GCSi-treated mouse brain were sensitive to SDS, whereas oligomers from CBE mice were more resistant, as shown by syn505 and syn303 reactivity (Fig. 3*F*). This suggests that reducing long-chain GluCers prevented the conversion into pathological-type α-syn oligomers in vivo. Consistent with this, we found a reduction in astrogliosis, as indicated by GFAP staining in the cortex of GCSi-treated mice (Fig. 3*G*). Together, these data suggest that coadministration of GCSi with CBE selectively prevents the accumulation of long-chain GluCers that are required to initiate α-syn oligomer conversion and neurotoxicity.

Reducing Long-Chain GluCers Can Reverse Preexisting α-syn Pathology In Vivo. We next sought to determine if reducing GluCer could rescue mice with preexisting α-syn pathology. Mice were treated with CBE alone for 7 d to induce α-syn pathology and neurotoxicity (as in Fig. 2), followed by an additional 7-d treatment of CBE + GCSi. Both CBE- and CBE + GCSi–treated mice showed an equal reduction in GCase activity (Fig. 4*A*), while GCSi treatment reduced long-chain GluCers by 30 to 40% in the cortex (Fig. 4*B*). Insoluble α-syn was reduced by similar degrees when analyzed with α-syn antibodies C20, syn303, and syn505 (Fig. 4*C*). Analysis of soluble oligomeric species showed a dramatic reduction in pathogenic species since most of the oligomers were eliminated by treating the lysate with SDS prior to SEC (Fig. 4*D*). Furthermore, astrogliosis was partially reduced and neurological function was improved, as assessed by rotarod tests (Fig. 4 *E* and *F*). Taken together, these data indicate that GCSi treatment can reduce both long-chain GluCer accumulation and reverse α-syn pathology in the brain, even when administered after mature aggregates are formed.

Long-Chain GluCers Directly Induce α-syn Aggregation. Since our data indicated a correlation between long-chain GluCers and α-syn aggregation in vivo, we next determined if long-chain GSLs could directly stimulate α-syn aggregation in cell culture models. C22 and C24 GSLs are synthesized in the Golgi from ceramides specifically produced by ceramide synthase 2 (CerS2). Therefore, we transfected cell lines with CerS2 plasmids to determine the effect of long-chain sphingolipids on α-syn aggregation. We found that CerS2 overexpression caused an accumulation of insoluble α-syn but did not alter soluble α-syn levels (Fig. 5*A*). Next, we added purified GluCer particles made from either C16 or C24 GluCer to the culture media to directly assess the effect of GluCer on α-syn. We employed a previously established protocol to generate aggregated GluCer tubules made of 75% GluCer and 25% phosphatidylcholine (PC) that are similar in structure to those found in GD (45). Immunofluorescence studies showed that exogenously applied, fluorescently labeled GluCer internalized into cells within 1 d and accumulated within LAMP1+ structures, consistent with late endosomes or lysosomes (Fig. 5*B*). Addition of C16 GluCer to healthy human midbrain neurons did not induce α-syn aggregation compared to nontreated or PC-treated controls; however, we observed a dramatic accumulation of insoluble α-syn upon treatment with C24 GluCer (Fig. 5 *C* and *D*). These data demonstrate that long-chain GluCers can directly initiate α-syn aggregation when exogenously applied to healthy human midbrain cultures.

Lysosomal Cathepsins Are Required to Clear Pathogenic α-syn. Since our data indicated that reducing long-chain GluCers reduces α-syn pathology in mice, we next sought to determine if similar changes could be observed in GD and PD patient midbrain neurons that develop α-syn inclusions in a chronic manner (38). We treated an established nGD patient midbrain line (*GBA1* N370S/c.84dupG) with the same GCSi, venglustat, that was used in our in vivo studies. A baseline comparison of nGD

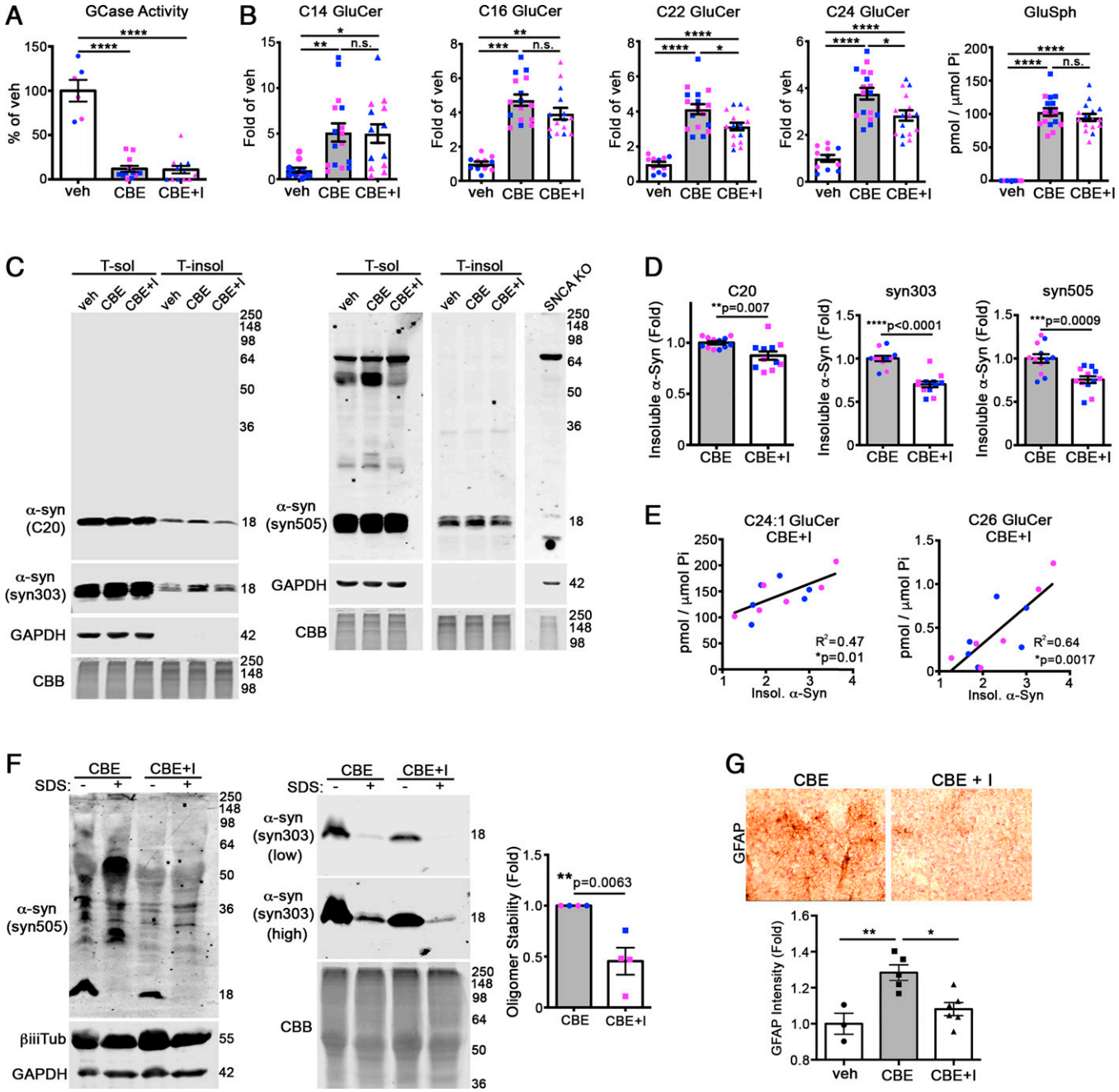

Fig. 3. Preventing the accumulation of long-chain GluCers reduces the formation of pathological α-syn aggregates in mouse brain. The 3-mo-old wt mice were simultaneously treated with CBE and venglustat, a glucosylceramide synthase inhibitor (I), for 7 d followed by analysis of cortex. (*A*) GCase activity was measured in cortical lysates, normalized to total protein, and expressed relative to vehicle (veh) control (n = 12 per group). (*B*) GluCers and GluSph from cortex were quantified by supercritical fluid chromatography (SFC)-mass spectrometry (MS)/MS analysis and normalized to inorganic phosphate (Pi) (n = 12 per group). (*C*) Cortex was sequentially extracted and separated into triton X-100 soluble (T-sol) and insoluble (T-insol) fractions followed by Western blot for α-syn. C20 (rabbit pAb) and syn303 (mouse mAb) were sequentially probed on the same blot and detected with distinct, fluorescent secondary antibodies. Syn505 is shown from a separate blot. GAPDH and Coomassie Brilliant Blue (CBB) were used as loading controls. Lysates from α-syn knock-out lines (*SNCA* KO) were used to validate antibody specificity. (*D*) Quantification of insoluble α-syn normalized to total protein (CBB stain) (n = 12 mice per group). (*E*) Correlation of high-chain GluCers C24:1 and C26 with insoluble α-syn detected with syn303. (*F*) T-sol lysates were treated with or without 0.1% SDS to reveal stable, pathogenic oligomers followed by SEC analysis, quantified to the right with syn505 normalized to CBB (n = 4). CBE + veh/CBE + I pairs were analyzed on separate blots, and CBE + veh was assigned as onefold for each analysis. (*G*) Immunohistochemical analysis of the cortex of treated mice reveals a reduction in GFAP staining, suggesting reduced neural injury at day 7 post-injection. Values are the mean ± SEM; Student's t test was used for *D* and *F*; ANOVA with Tukey's post hoc test was used for *A*, *B*, and *G*; $^*P < 0.05$, $^{**}P < 0.01$, $^{***}P < 0.001$, and $^{****}P < 0.0001$. N.S., not significant.

midbrain cultures compared to wt healthy controls showed that short-chain GluCers (C14 and C16) were not different, while long-chain GluCers of C20, C22, and C24 chain lengths showed the most dramatic elevation of four- to sixfold (Fig. 6*A*). Analysis of ceramide indicated no change in GD lines (Fig. 6*A*). GCSi reduced total GluCers but, more importantly, could reduce the accumulation of long-chain forms C22 and C24 (Fig. 6*B*). Similar to our previous studies (22), GCSi treatment

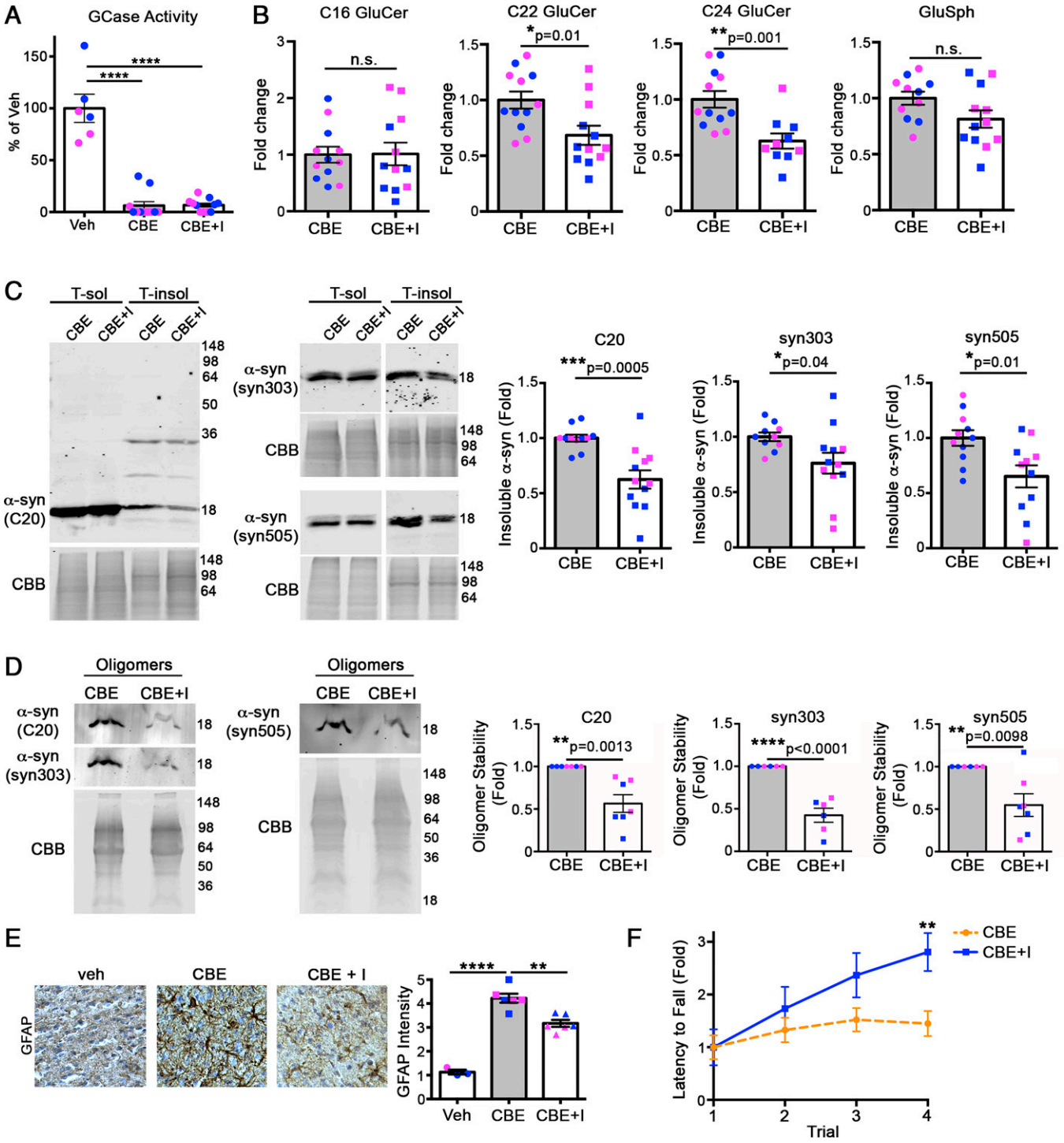

Fig. 4. Reduction of long-chain GluCers rescues α-syn pathology in CBE-injected mice. The 3-mo-old wt mice were sequentially treated with CBE alone for 7 d, followed by CBE and venglustat, a glucosylceramide synthase inhibitor (I), for an additional 7 d. Cortex was then harvested and analyzed. (*A*) GCase activity was measured in cortical lysates, normalized to total protein, and expressed relative to vehicle (veh) control ($n = 12$ per group). (*B*) GluCers and GluSph from cortex were quantified by supercritical fluid chromatography (SFC)-mass spectrometry (MS)/MS analysis and normalized to inorganic phosphate (Pi) ($n = 12$ per group). (*C*) Cortex was sequentially extracted and separated into triton X-100 soluble (T-sol) and insoluble (T-insol) fractions followed by Western blot for α-syn. GAPDH and Coomassie Brilliant Blue (CBB) were used as loading controls. Quantifications are shown on the right. (*D*) Quantification of pathogenic α-syn oligomers by SEC/Western blot. T-sol lysates were treated with 0.1% SDS to reveal stable, pathogenic oligomers followed by SEC analysis, quantified to the right ($n = 6$ to 7). C20 (rabbit pAb) and syn303 (mouse mAb) were sequentially probed on the same blot and detected with distinct, fluorescent secondary antibodies. Syn505 is shown on a separate blot. (*E*) Immunohistochemical analysis of cortical regions of treated mice reveals a reduction in GFAP staining, suggesting reduced neural injury at day 14 post-injection. Values are the mean ± SEM, Student's *t* test; $^{*}P < 0.05$, $^{**}P < 0.01$, $^{***}P < 0.001$, and $^{****}P < 0.0001$. Each plot shown represents an individual mouse (pink, female; blue, male). (*F*) Rotarod performance was tested at day 14 in mice injected with either CBE alone or CBE + venglustat ($n = 4$). Values are the mean ± SEM; Student's *t* test was used for *B–D*, and *F*; ANOVA with Tukey's post hoc test was used for *A* and *E*; $^{*}P < 0.05$, $^{**}P < 0.01$, $^{***}P < 0.001$, and $^{****}P < 0.0001$. N.S., not significant.

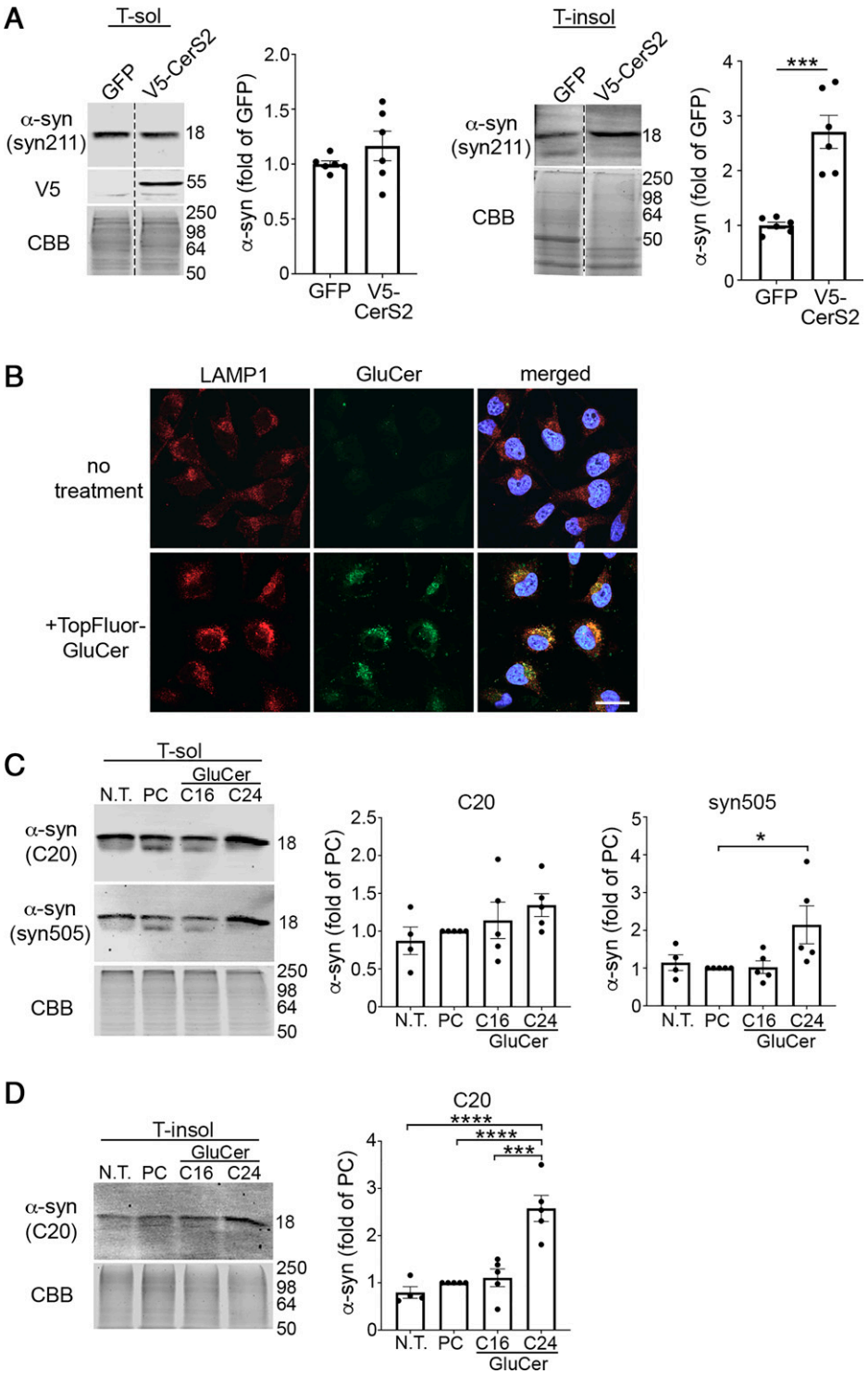

Fig. 5. Long-chain GSLs induce α-syn pathology in a human cell line and iPSC-derived midbrain neurons. (*A*) H4 cells were transfected with V5-tagged CerS2 followed by sequential extraction/Western blot to quantify insoluble α-syn ($n = 6$). (*B*) Fluorescent-labeled (TopFluor) GluCer (100 μm) was added to H4 cells that overexpress α-syn and uptake was analyzed by confocal microscopy of fixed cells 1 d later. Localization within lysosomes was assessed by LAMP1 immunofluorescence. Nuclei (DAPI) are shown in blue. (Scale bar, 25 μm.) (*C* and *D*) iPSC-derived midbrain cultures from healthy subjects aged to day 170 were cultured with 100 μM C16 or C24 GluCer for 3 d followed by sequential extraction and separated into triton X-100 soluble (T-sol) (*C*) and insoluble (T-insol) (*D*) lysates followed by Western blot to quantify aggregated α-syn. In *C*, C20 (rabbit pAb) and syn505 (mouse mAb) were sequentially probed on the same blot and detected with distinct, fluorescent secondary antibodies. Neurons were either not treated (N.T.) or cultured with equimolar PC as controls ($n = 5$). Values are the mean ± SEM; Student's *t* test was used for *B*; ANOVA with Tukey's post hoc test was used for *C* and *D*; $^{*}P < 0.05$, $^{***}P < 0.001$, and $^{****}P < 0.0001$.

https://doi.org/10.1073/pnas.2108489118

did not change the total levels of soluble α-syn but reduced insoluble forms by ∼60% (Fig. 6*C*). We found a similar effect when other culture models were treated with GCSi including GD neurons that express L444P/L444P GCase (Fig. 6*D*), as well as idiopathic PD and GBA-PD (N370S/wt) neurons that were aged to 9 mo (*SI Appendix*, Fig. S3). These data indicate that reducing long-chain GSLs could benefit both severe GD patients and milder, chronic cases of PD.

We next utilized midbrain culture models to gain insight into the mechanism of α-syn clearance when treated with GCSi. Our in vivo studies indicated that lowering GluCers reduced the stability of oligomeric α-syn, suggesting that oligomers could be more susceptible to degradation by lysosomal proteases. Previous studies also suggested that α-syn could be cleared by lysosomal cathepsins (12), and mutations in *CTSB* have recently been linked to GBA-PD as a potential disease modifier (8). Furthermore, our studies in healthy wt control neurons indicate that insoluble α-syn accumulates upon lysosomal inhibition with the broad cathepsin inhibitor leupeptin, as well as with *CTSB* knock-down (KD) by short hairpin RNA (shRNA) (*SI Appendix*, Fig. S4). This suggests that α-syn is normally degraded through lysosomes in human midbrain cultures, consistent with previous findings (9). We inhibited lysosomal cathepsins with leupeptin, macroautophagy with 3-methyladenine (3-MA), and the proteasome with epoxomicin (Epox), along with GCSi treatment. GCSi treatment potently reduced insoluble α-syn even in the presence of 3-MA or Epox, suggesting that macroautophagy or the proteasome are not involved in α-syn clearance (Fig. 6*C*). However, leupeptin treatment abolished the ability of GCSi to reduce α-syn (Fig. 6*C*). This result was confirmed in a distinct nGD line expressing L444P/L444P GCase (Fig. 6*D*) (28).

Since cathepsin B cleaves α-syn in the Non-A-beta Component (NAC) region (12) and has been genetically linked to GBA-PD (8), we next determined if more specific inhibitors could prevent α-syn clearance when patient cultures are treated with GCSi. We treated cultures with CA-074Me, an inhibitor of cathepsins B and L, or MDL 28170 that inhibits both cathepsin B and calpain. We found that both inhibitors prevented GCSi-mediated clearance of insoluble α-syn in two different patient GD midbrain lines (Fig. 6 *E* and *F*). To confirm these results, we infected GD neurons with lenti-*CTSB* shRNA constructs, followed by treatment with GCSi for 14 d. We found that *CTSB* KD significantly impeded the clearance of α-syn in GCSi-treated cultures (Fig. 6*G*). GCSi was still capable of reducing α-syn in *CTSB* KD neurons by ∼30%, which could be due to the incomplete KD of *CTSB* or from the contribution of other cathepsins. Finally, we tested the effect of *CTSB* overexpression in an α-syn–overexpressing H4 cell line. While CBE treatment increased the levels of α-syn in vector-transfected cells as expected, *CTSB* overexpression prevented CBE-induced α-syn accumulation (*SI Appendix*, Fig. S5). Together, this indicates that lysosomal cathepsin B is critical in clearing pathogenic α-syn in patient neurons upon GSL reduction.

Discussion

Our studies uncover unexpected, complex features of the mechanistic relationship between GCase and α-syn that extends beyond simple loss of GCase activity and α-syn aggregation. We find that GSL accumulation does not invariably lead to α-syn aggregation but depends on neuronal maturity and the physiological conformation of α-syn in vivo, fatty-acyl chain length of GluCers, and lysosomal cathepsins. Neonatal mouse brain or immature human neurons predominantly express monomers and were surprisingly resistant to GSL-induced α-syn aggregation (Fig. 1). While other factors could contribute to the resistance of α-syn aggregation in immature neurons, we show that the total α-syn levels or reduced lysosomal activity likely do not contribute (*SI Appendix*, Fig. S1). Furthermore, our previous studies using nGD patient midbrain cultures and isolated α-syn species in vitro showed that GSLs directly stimulate soluble oligomers into forming insoluble aggregates, with little effect on monomers (22). Our studies on mouse brain further supports the hypothesis that preexisting, physiological oligomers promote α-syn aggregation when GSLs are elevated in vivo. It is possible that α-syn oligomers documented here represent prenucleus species that exist in brain and convert into aggregation-competent oligomers upon interaction with GSLs, as previously shown in patient iPSC neurons (22). nGD or GBA-PD patients may express particularly high levels of physiological oligomers at baseline prior to disease onset, while those *GBA1* carriers that are protected from neurological symptoms have lower-baseline levels of oligomers. Similarly, circumscribed regions of GBA-PD brain that exhibit Lewy pathology, including cortex, midbrain, and hippocampus, may contain higher-oligomer/monomer ratios, as compared to other pathology-free brain regions, rendering these neuronal subtypes vulnerable to α-syn aggregation. The physiological function of α-syn oligomers is not clear; however, previous work suggests that α-syn can multimerize into oligomeric species at synapses under physiological conditions and promote SNARE assembly (46). α-syn exhibits homology with exchangeable apolipoproteins and binds acidic phospholipids that share similarities with synaptic vesicles (47). It is possible that α-syn monomers coalesce on membrane structures, including synaptic vesicles, to form physiological oligomers. The factors that control the formation of physiological α-syn oligomers are not known; however, they could be related to neural activity, given their putative role in synaptic transmission. Future studies comparing α-syn conformers of nonsymptomatic *GBA1* carriers with those from PD/Dementia with Lewy Bodies (DLB) should further provide insight into their role in pathogenesis. Similarly, comparing the distribution and expression levels of α-syn conformers within disease brain may lead to mechanistic clues to explain the selective vulnerability of midbrain and cortical neurons.

We found that long-chain GSLs (≥C22) were strongly correlated with α-syn pathology in vivo. Reducing long-chain GluCers with GCSi, while short-chain species remained elevated, was sufficient to reduce α-syn pathology and partially reduce neuroinflammation (Figs. 3 and 4). GCSi inhibits GCS in the Golgi and should theoretically inhibit the synthesis of all GluCer species equally. We observed a selective reduction of long-chain GluCers in vivo consistent with previous observations (43), but the reasons for this selective reduction are not known. It may be due to baseline differences in synthesis, transport, turnover rates of distinct ceramides, or GluCer species within cells that allow for longer-chain GluCer species to be more dramatically affected by GCSi. Variable efficiency of the GCSi within certain cell types that predominantly express long-chain GluCers may also contribute. For example, it is known that CerS2 is highly expressed in oligodendroglia but is also prominently expressed in certain neuronal subtypes of the cortex and hippocampus (48).

Our in vitro mechanistic studies further emphasized the importance of long-chain GluCers in pathogenesis, since exogenous addition of C24 but not C16 GluCer could directly induce α-syn aggregation in healthy iPSC–midbrain cultures (Fig. 5). Our previous studies indicated that GluCer can directly interact with α-syn in vitro and colocalizes with α-syn in lysosomes of midbrain neurons (22, 45). It is likely that pathogenic microenvironments within the cell contain elevated concentrations of long-chain GSLs and α-syn oligomers that surpass the threshold to induce aggregation. If concentrations are high enough,

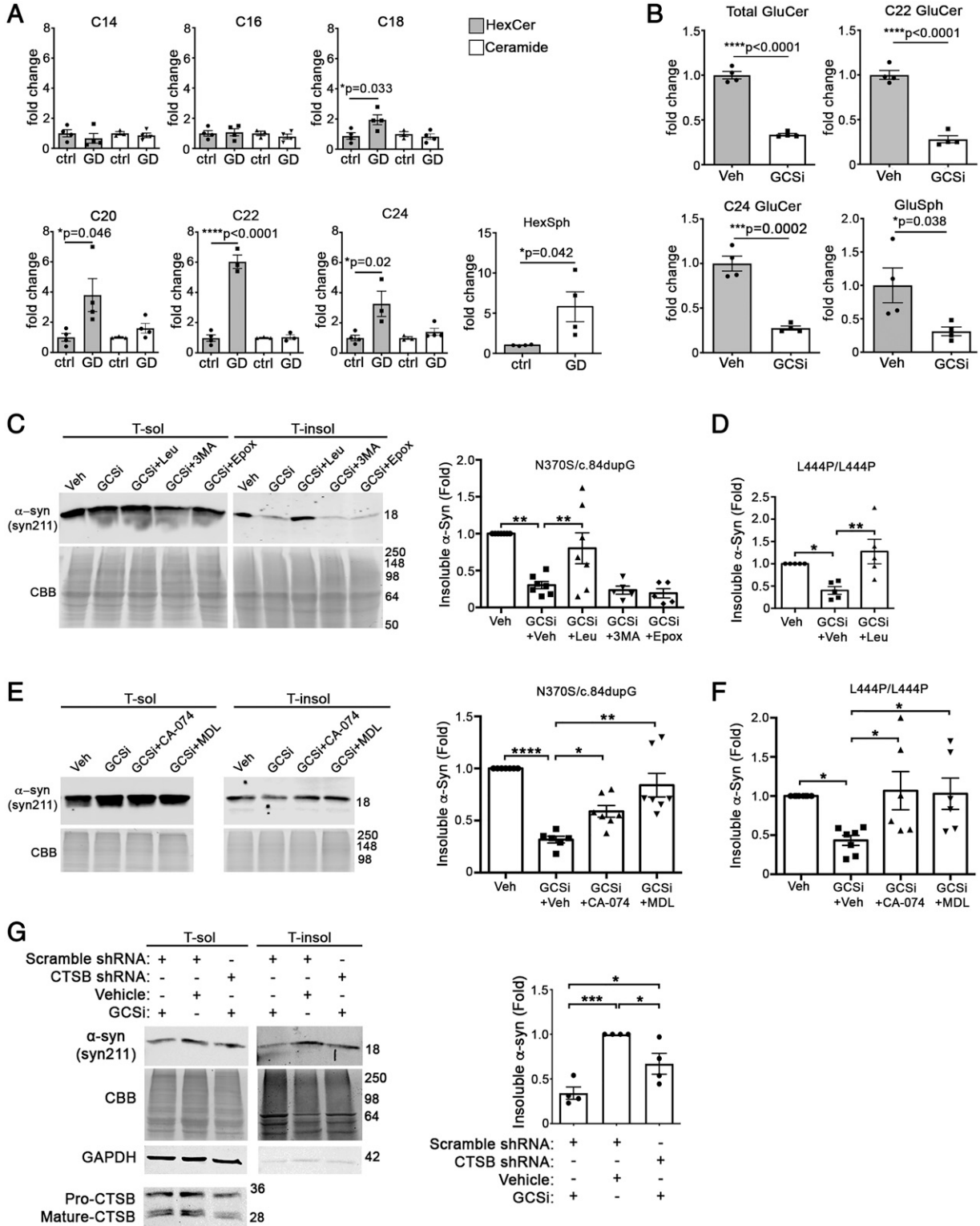

Fig. 6. Long-chain GluCers selectively accumulate in nGD patient midbrain cultures, and their reduction lowers α-syn in a cathepsin-dependent manner. (*A*) Lipidomic analysis reveals accumulation of long-chain GluCers in GD neurons expressing N370S/c.dup84GG (n = 3 to 4 culture wells). (*B*) Treatment of GD midbrain cultures with 50 nM venglustat (GCSi) reduces long-chain GluCers and GluSph. (*C*) iPSCs from nGD patients were treated with venglustat and proteolytic inhibitors, and then analyzed at day 75. Sequential extraction/Western blot of iPSC–midbrain cultures from GD patients expressing N370S/c.84dupG mutations were treated with GCSi and inhibitors of lysosomal cathepsins (Leupeptin, Leu), macroautophagy (3-MA), or the proteasome (Epox). (*D*) iPSC–midbrain cultures from nGD patients expressing L444P/L444P mutations were analyzed as in *C*. (*E*) GD neurons expressing N370S/c.84dupG mutations were treated with GCSi and specific inhibitors of lysosomal cathepsins, including CA-074Me (cathepsin B + L) and MDL 28170 (cathepsin B and calpain). (*F*) nGD neurons expressing L444P/L444P were analyzed as in *E*. (*G*) GD midbrain neurons expressing N370S/c.84dupG mutations were treated with lentiviral shRNA particles to knock down CTSB and then 2 d later were treated with 50 nM venglustat for 14 d. Cultures were analyzed as in *C*. Values are the mean ± SEM; unpaired Student's *t* test was used for *A* and *B*; ANOVA with Tukey's post hoc test was used for *C*–*G*; $^*P < 0.05$, $^{**}P < 0.01$, $^{***}P < 0.001$, and $^{****}P < 0.0001$.

GSLs can segregate into aggregated gel domains within local microenvironments of lipid bilayers (49) and accumulate within lipid rafts, as shown in GD models (50, 51). Lipid rafts are internalized and degraded through the endolysosomal system (52), and α-syn is also known to be trafficked to lysosomes for degradation (9), indicating that pathogenic microenvironments may form within the endolysosomal system. Long-chain lipid species may be particularly vulnerable to accumulation or promoting α-syn conversion when trafficked to lysosomes, since the extended fatty acyl chain and hydrophobic interactions may promote lipid–lipid or lipid–protein aggregation. Insertion of long-chain sphingolipids into phospholipid biolayers alters their rigidity and can induce the formation of protruding lipid tubules or ribbons (49, 53–55). These structures may provide an optimal, nucleating surface to convert α-syn into pathogenic species within subcellular compartments. It is possible that patients with nGD or GBA-PD produce elevated levels of long-chain GluCers, for example, through increased activity of CerS2, rendering them susceptible to α-syn–induced neurodegeneration. Interestingly, the expression pattern of CerS2 in the brain is somewhat selective, with expression shown in oligodendroglia of white matter tracts, as well as in neurons of the cortex, midbrain, and circumscribed areas of the hippocampus (48). Our studies show that CerS2 is expressed in human midbrain cultures made from iPSCs (*SI Appendix*, Fig. S6) that are mainly comprised of β-iii-tubulin + neurons. Long-chain GluCers also selectively accumulate in nGD midbrain cultures (Fig. 6*A*), suggesting that cell-autonomous mechanisms may play a role. However, the high expression of CerS2 and concentration of long-chain GluCers in glial cells indicates the possibility that neuron–glia interaction may also contribute to α-syn pathology in vivo.

Previous studies have shown that GluCer accumulation occurs in the brains of patients with nGD, both within neurons and in perivascular macrophages (15–19). Ultrastructural studies of GD mouse models show that GluCer accumulates within neurons, and analysis of whole-cell extracts shows both short- and long-chain-length species accumulate (14). In PD patients, some studies have shown that GSLs do not accumulate in brain, while others have documented reduced GCase activity and GSL elevation in certain brain regions (56, 57). Although informative, previous studies did not assess the cellular topology or concentrations of GSLs within subcellular microenvironments, and cell-type–specific changes in GSLs have not been examined. Technical limitations in the extraction process, involving tissue destruction and whole-cell lysis, does not permit the selective measurement of GSLs within certain cell types, such as neurons, or subcellular compartments of the endolysosomal system where pathogenic microenvironments are expected to occur. Such measurements, along with chain length analysis, would provide better resolution into the pathogenic alterations that occur in GD and PD brain. For example, previous studies have documented GluCer accumulation in homogenous populations of PD patient midbrain cultures that express either wt GCase or heterozygote *GBA1* carriers (21, 28, 38). In addition to the total steady-state levels of GluCers in the cell, the flux rate and trafficking of GluCers between subcellular compartments is also likely to play an important role in α-syn aggregation. For example, it is known that long-chain GluCers such as C24 are also trafficked more slowly in vitro (58). Slowed movement of long-chain GluCers may allow for more opportunities to interact with α-syn in the cell, promoting the conversion into protein aggregates.

The advantages of the CBE model include a robust and reproducible accumulation of brain GSLs that occurs within 7 d, which facilitates the biochemical study of GSL-induced α-syn aggregation. As a highly dynamic protein, examining α-syn aggregation kinetics in vivo requires precise temporal control over the initiation of the process so that distinct conformations can be followed over time. The model also achieves a near-complete reduction in GCase activity, which is similar to nGD but distinct from GBA-PD where 50% of the activity remains. The changes documented here apply to GD but also recapitulate some features of GBA-PD, given the similarities at the end stage of disease, including insoluble α-syn aggregates, neuroinflammation, and motor behavior deficits. The CBE model may represent an accelerated version of the pathological aggregation process that likely occurs over several decades in GBA-PD. However, since CBE provides a systemic reduction of GCase activity in the periphery as well as the central nervous system, some of the behavioral and histological changes we observe could be due to indirect effects that occur in the periphery. Future in-depth studies that comprehensively examine neurodegeneration will provide greater insight into the relationship between systemic effects and direct changes in the brain.

Our data also indicates that lysosomal cathepsins are required to degrade α-syn, when GSLs are reduced by GCSi treatment. This has important implications for the therapeutic development of nGD and GBA-PD. Our data predicts that these patients may not benefit from GCSi treatment unless lysosomal cathepsins are fully functional. Therefore, patients with potentially damaging single-nucleotide polymorphisms (SNPs) in cathepsins may not benefit from a GCSi or other GSL-reducing therapies. Conversely, patients with fully functional cathepsins or protective SNPs that enhance cathepsin activity may benefit from GCSi or, possibly, not develop neuronopathic phenotypes in the first place, given that lysosomes would be capable of degrading α-syn during the earliest stages of the aggregation process. This information may provide guidance that could optimize *GBA1* patient selection for future clinical trials.

In summary, our data indicate that the pathogenesis of *GBA1* mutations extends beyond reduced GCase activity and GSL accumulation. The neuronopathic phenotype is influenced by additional factors identified here, and it is likely that other genetic and nongenetic modifiers will be subsequently discovered. Future work that focuses on comparing the physiological conformers of α-syn, lipidomic profiles, and lysosomal cathepsin activity of patient samples from asymptomatic and nGD should provide critical insight into the mechanisms of *GBA1*-induced neurodegeneration.

Materials and Methods

Further information and request for resources should be made to J.R.M. at jmazzulli@northwestern.edu. Raw western blot data has been deposited online at Mendeley Data: http://doi.org/10.17632/nwf89s4y8p.1.

Treatment and Analysis of CBE Mice. The wt C57BL/6 mice (strain code 027) were injected i.p. daily for 7 to 14 d with CBE (Sigma-Aldrich C5424) at 100 mg/kg starting at P8 or 3 mo of age, as indicated in the text. Tissues were harvested and analyzed by histological and biochemical methods as indicated in *SI Appendix*.

Cell Culture Experiments. iPSCs from patients and controls were cultured and differentiated into midbrain neurons as previously described (38). Cultures were matured for various times depending on the experiment (30, 90, 120, or 270 d), as indicated in the text. Cultures were analyzed by biochemical techniques as indicated in *SI Appendix*.

Data Availability. All study data are included in the article and/or *SI Appendix*. Raw western blot data has been deposited online at Mendeley Data: http://doi.org/10.17632/nwf89s4y8p.1.

ACKNOWLEDGMENTS. This work was supported by the National Institute of Neurological Disorders and Stroke of the NIH under Award No. RF1NS109157 (J.R.M.) and the Michael J. Fox Foundation under Award No. 12158 (J.R.M.). This work was supported in part by the Lipidomics Shared Resource, Hollings Cancer Center, Medical University of South Carolina (P30 CA138313 and P30 GM103339)

1. I. Stojkovska, D. Krainc, J. R. Mazzulli, Molecular mechanisms of alpha-synuclein and GBA1 in Parkinson's disease. *Cell Tissue Res.* **373**, 51–60 (2018).
2. G. A. Grabowski, Phenotype, diagnosis, and treatment of Gaucher's disease. *Lancet* **372**, 1263–1271 (2008).
3. K. Wong *et al.*, Neuropathology provides clues to the pathophysiology of Gaucher disease. *Mol. Genet. Metab.* **82**, 192–207 (2004).
4. C. Pitcairn, W. Y. Wani, J. R. Mazzulli, Dysregulation of the autophagic-lysosomal pathway in Gaucher and Parkinson's disease. *Neurobiol. Dis.* **122**, 72–82 (2019).
5. G. Bultron *et al.*, The risk of Parkinson's disease in type 1 Gaucher disease. *J. Inherit. Metab. Dis.* **33**, 167–173 (2010).
6. C. K. Zhang *et al.*, Genome-wide association study of N370S homozygous Gaucher disease reveals the candidacy of CLN8 gene as a genetic modifier contributing to extreme phenotypic variation. *Am. J. Hematol.* **87**, 377–383 (2012).
7. A. Velayati *et al.*, A mutation in SCARB2 is a modifier in Gaucher disease. *Hum. Mutat.* **32**, 1232–1238 (2011).
8. C. Blauwendraat *et al.*, 23andMe Research Team, Genetic modifiers of risk and age at onset in GBA associated Parkinson's disease and Lewy body dementia. *Brain* **143**, 234–248 (2020).
9. A. M. Cuervo, L. Stefanis, R. Fredenburg, P. T. Lansbury, D. Sulzer, Impaired degradation of mutant alpha-synuclein by chaperone-mediated autophagy. *Science* **305**, 1292–1295 (2004).
10. J. L. Webb, B. Ravikumar, J. Atkins, J. N. Skepper, D. C. Rubinsztein, α-synuclein is degraded by both autophagy and the proteasome. *J. Biol. Chem.* **278**, 25009–25013 (2003).
11. D. Ebrahimi-Fakhari *et al.*, Distinct roles in vivo for the ubiquitin-proteasome system and the autophagy-lysosomal pathway in the degradation of α-synuclein. *J. Neurosci.* **31**, 14508–14520 (2011).
12. R. P. McGlinchey, J. C. Lee, Cysteine cathepsins are essential in lysosomal degradation of α-synuclein. *Proc. Natl. Acad. Sci. U.S.A.* **112**, 9322–9327 (2015).
13. P. S. Sastry, Lipids of nervous tissue: Composition and metabolism. *Prog. Lipid Res.* **24**, 69–176 (1985).
14. T. Farfel-Becker *et al.*, Neuronal accumulation of glucosylceramide in a mouse model of neuronopathic Gaucher disease leads to neurodegeneration. *Hum. Mol. Genet.* **23**, 843–854 (2014).
15. N. G. Conradi, P. Sourander, O. Nilsson, L. Svennerholm, A. Erikson, Neuropathology of the Norrbottnian type of Gaucher disease. Morphological and biochemical studies. *Acta Neuropathol.* **65**, 99–109 (1984).
16. M. Sudo, Brain glycolipids in infantile Gaucher's disease. *J. Neurochem.* **29**, 379–381 (1977).
17. E. M. Kaye, M. D. Ullman, E. R. Wilson, J. A. Barranger, Type 2 and type 3 Gaucher disease: A morphological and biochemical study. *Ann. Neurol.* **20**, 223–230 (1986).
18. M. Grafe, C. Thomas, J. Schneider, B. Katz, C. Wiley, Infantile Gaucher's disease: A case with neuronal storage. *Ann. Neurol.* **23**, 300–303 (1988).
19. E. E. Jones *et al.*, Tissue localization of glycosphingolipid accumulation in a Gaucher disease mouse brain by LC-ESI-MS/MS and high-resolution MALDI imaging mass spectrometry. *SLAS Discov.* **22**, 1218–1228 (2017).
20. T. A. Burrow *et al.*, CNS, lung, and lymph node involvement in Gaucher disease type 3 after 11 years of therapy: Clinical, histopathologic, and biochemical findings. *Mol. Genet. Metab.* **114**, 233–241 (2015).
21. L. K. Cuddy *et al.*, Stress-induced cellular clearance is mediated by the SNARE protein ykt6 and disrupted by α-Synuclein. *Neuron* **104**, 869–884.e11 (2019).
22. F. Zunke *et al.*, Reversible conformational conversion of α-synuclein into toxic assemblies by glucosylceramide. *Neuron* **97**, 92–107.e10 (2018).
23. S. P. Sardi *et al.*, Glucosylceramide synthase inhibition alleviates aberrations in synucleinopathy models. *Proc. Natl. Acad. Sci. U.S.A.* **114**, 2699–2704 (2017).
24. S. Kim *et al.*, GBA1 deficiency negatively affects physiological α-synuclein tetramers and related multimers. *Proc. Natl. Acad. Sci. U.S.A.* **115**, 798–803 (2018).
25. G. Dermentzaki, E. Dimitriou, M. Xilouri, H. Michelakakis, L. Stefanis, Loss of β-glucocerebrosidase activity does not affect alpha-synuclein levels or lysosomal function in neuronal cells. *PLoS One* **8**, e60674 (2013). Correction in: *PLoS One* **16**, e0252975 (2021).
26. M. X. Henderson *et al.*, Glucocerebrosidase activity modulates neuronal susceptibility to pathological α-synuclein insult. *Neuron* **105**, 822–836.e7 (2020).
27. Y. H. Xu *et al.*, Accumulation and distribution of alpha-synuclein and ubiquitin in the CNS of Gaucher disease mouse models. *Mol. Genet. Metab.* **102**, 436–447 (2011).
28. D. C. Schöndorf *et al.*, iPSC-derived neurons from GBA1-associated Parkinson's disease patients show autophagic defects and impaired calcium homeostasis. *Nat. Commun.* **5**, 4028 (2014).
29. A. B. Manning-Boğ, B. Schüle, J. W. Langston, Alpha-synuclein-glucocerebrosidase interactions in pharmacological Gaucher models: A biological link between Gaucher disease and parkinsonism. *Neurotoxicology* **30**, 1127–1132 (2009).
30. E. M. Rocha *et al.*, Sustained systemic glucocerebrosidase inhibition induces brain α-synuclein aggregation, microglia and complement C1q activation in mice. *Antioxid. Redox Signal.* **23**, 550–564 (2015).
31. M. W. J. Cleeter *et al.*, Glucocerebrosidase inhibition causes mitochondrial dysfunction and free radical damage. *Neurochem. Int.* **62**, 1–7 (2013).
32. J. N. Kanfer, G. Legler, J. Sullivan, S. S. Raghavan, R. A. Mumford, The Gaucher mouse. *Biochem. Biophys. Res. Commun.* **67**, 85–90 (1975).
33. Y.-H. Xu *et al.*, Dependence of reversibility and progression of mouse neuronopathic Gaucher disease on acid beta-glucosidase residual activity levels. *Mol. Genet. Metab.* **94**, 190–203 (2008).
34. A. Vardi *et al.*, Delineating pathological pathways in a chemically induced mouse model of Gaucher disease. *J. Pathol.* **239**, 496–509 (2016).
35. S. J. Wood *et al.*, alpha-synuclein fibrillogenesis is nucleation-dependent. Implications for the pathogenesis of Parkinson's disease. *J. Biol. Chem.* **274**, 19509–19512 (1999).
36. B. I. Giasson, K. Uryu, J. Q. Trojanowski, V. M. Lee, Mutant and wild type human alpha-synucleins assemble into elongated filaments with distinct morphologies in vitro. *J. Biol. Chem.* **274**, 7619–7622 (1999).
37. A. B. Singleton *et al.*, alpha-synuclein locus triplication causes Parkinson's disease. *Science* **302**, 841 (2003).
38. J. R. Mazzulli, F. Zunke, O. Isacson, L. Studer, D. Krainc, α-Synuclein-induced lysosomal dysfunction occurs through disruptions in protein trafficking in human midbrain synucleinopathy models. *Proc. Natl. Acad. Sci. U.S.A.* **113**, 1931–1936 (2016).
39. R. Kayed *et al.*, Common structure of soluble amyloid oligomers implies common mechanism of pathogenesis. *Science* **300**, 486–489 (2003).
40. A. Laganowsky *et al.*, Atomic view of a toxic amyloid small oligomer. *Science* **335**, 1228–1231 (2012).
41. J. C. Stroud, C. Liu, P. K. Teng, D. Eisenberg, Toxic fibrillar oligomers of amyloid-β have cross-β structure. *Proc. Natl. Acad. Sci. U.S.A.* **109**, 7717–7722 (2012).
42. K. M. Ashe *et al.*, Efficacy of enzyme and substrate reduction therapy with a novel antagonist of glucosylceramide synthase for Fabry disease. *Mol. Med.* **21**, 389–399 (2015).
43. J. Marshall *et al.*, CNS-accessible inhibitor of glucosylceramide synthase for substrate reduction therapy of neuronopathic gaucher disease. *Mol. Ther.* **24**, 1019–1029 (2016).
44. J. E. Duda, B. I. Giasson, M. E. Mabon, V. M.-Y Lee, J. Q. Trojanowski, Novel antibodies to synuclein show abundant striatal pathology in Lewy body diseases. *Ann. Neurol.* **52**, 205–210 (2002).
45. J. R. Mazzulli *et al.*, Gaucher disease glucocerebrosidase and α-synuclein form a bidirectional pathogenic loop in synucleinopathies. *Cell* **146**, 37–52 (2011).
46. J. Burré, M. Sharma, T. C. Südhof, α-synuclein assembles into higher-order multimers upon membrane binding to promote SNARE complex formation. *Proc. Natl. Acad. Sci. U.S.A.* **111**, E4274–E4283 (2014).
47. D. F. Clayton, J. M. George, Synucleins in synaptic plasticity and neurodegenerative disorders. *J. Neurosci. Res.* **58**, 120–129 (1999).
48. S. Imgrund *et al.*, Adult ceramide synthase 2 (CERS2)-deficient mice exhibit myelin sheath defects, cerebellar degeneration, and hepatocarcinomas. *J. Biol. Chem.* **284**, 33549–33560 (2009).
49. A. R. P. Varela *et al.*, Effect of glucosylceramide on the biophysical properties of fluid membranes. *Biochim. Biophys. Acta* **1828**, 1122–1130 (2013).
50. L. K. Hein, S. Duplock, J. J. Hopwood, M. Fuller, Lipid composition of microdomains is altered in a cell model of Gaucher disease. *J. Lipid Res.* **49**, 1725–1734 (2008).
51. L. K. Hein, T. Rozaklis, M. K. Adams, J. J. Hopwood, L. Karageorgos, Lipid composition of microdomains is altered in neuronopathic Gaucher disease sheep brain and spleen. *Mol. Genet. Metab.* **121**, 259–270 (2017).
52. H. Schulze, T. Kolter, K. Sandhoff, Principles of lysosomal membrane degradation: Cellular topology and biochemistry of lysosomal lipid degradation. *Biochim. Biophys. Acta* **1793**, 674–683 (2009).
53. R. E. Lee, The fine structure of the cerebroside occurring in Gaucher's disease. *Proc. Natl. Acad. Sci. U.S.A.* **61**, 484–489 (1968).
54. S. N. Pinto, L. C. Silva, A. H. Futerman, M. Prieto, Effect of ceramide structure on membrane biophysical properties: The role of acyl chain length and unsaturation. *Biochim. Biophys. Acta* **1808**, 2753–2760 (2011).
55. A. R. P. Varela *et al.*, Pathological levels of glucosylceramide change the biophysical properties of artificial and cell membranes. *Phys. Chem. Chem. Phys.* **19**, 340–346 (2016).
56. E. M. Rocha *et al.*, Progressive decline of glucocerebrosidase in aging and Parkinson's disease. *Ann. Clin. Transl. Neurol.* **2**, 433–438 (2015).
57. M. E. Gegg *et al.*, No evidence for substrate accumulation in Parkinson brains with GBA mutations. *Mov. Disord.* **30**, 1085–1089 (2015).
58. A. P. E. Backman *et al.*, Glucosylceramide acyl chain length is sensed by the glycolipid transfer protein. *PLoS One* **13**, e0209230 (2018).